# Structural and Physico-Chemical Study of New Keggin Polyoxometalates with Mixed Adenda

**ANDA IOANA GRATIELA PETREHELE[1]*, DAN RUSU[2], ALIA UNGUREAN[3], GRAZIELLA L. TURDEAN[4], EMIL INDREA[5], LEONTIN DAVID[3], MARIANA RUSU[4]**

[1]University of Oradea, Department of Chemistry, 1 Universitãii Str., 410087, Oradea, Romania

[2]Medicine and Pharmacy „Iuliu Haeganu" University, Department of Physical Chemistry, 13 Emil Isac Str., 400023, Cluj-Napoca, Romania

[3]"Babes-Bolyai" University, Department of Physics, 1 Mihail Kogalniceanu, 400074, Cluj-Napoca, Romania

[4]"Babes-Bolyai" University, Faculty of Chemistry and Chemical Engineering, 11 Arany Janos Str., 400028, Cluj-Napoca, Romania

[5] National Institute for Research and Development of Isotopic and Molecular Technologies, Department of Physics of Nanostructured Systems Cluj-Napoca, 400293, Romania

*Reactions between $[\alpha\text{-}PVMo_{10}O_{39}]^{8-}$, mono-lacunary Keggin monovanado-deca-molybdophosphate and transition metal cations $Mn^{2+}$, $Fe^{3+}$, $Co^{2+}$, $Ni^{2+}$ and $Cu^{2+}$ in aqueous solution results in the formation of new polyoxometalate complexes, with the stoichiometry metal : ligand by 1:1. New complexes were isolated as potassium salts, i.e. $K_{8-n}[M^{n+}(H_2O)PVMo_{10}O_{39}] \cdot xH_2O$. The molecular formula of complexes was determined by elemental and thermo-gravimetric analysis, UV-Vis, FT-IR, Raman, EPR spectroscopy and X-ray diffraction. The investigation results strongly suggest a Keggin-type structure with mixed addenda of new complexes in which the transition metal cations are coordinated by five oxygen atoms of the cavity of lacunary polyoxometalate anions and sixth oxygen atom originates in the water molecule in distorted Oh symmetry. Some of new complexes, $K_6[Ni(H_2O)PVMo_{10}O_{39}] \cdot x\,H_2O$ ($x = 16, 21$) and $K_6[Cu(H_2O)PVMo_{10}O_{39}] \cdot 17H_2O$, crystallized in monoclinic system, space group $P2_1/c$. The electrocatalytic activity of the $K_6[Cu(H_2O)PVMo_{10}O_{39}] \cdot 17H_2O$ compound towards $H_2O_2$ was evidenced.*

*Keywords: Keggin polyoxometalates, FTIR, Raman, EPR spectroscopy, Cyclic voltammetry*

Polyoxometalates (POMs) are metal-oxygen clusters that exhibit a fascinating variety of structures and properties, including size, shape, charge, density, acidity, redox states, stability, solubility, etc. Transition metal substituted polyoxometalates (TMSPs) have attracted a continually growing interest in the field of polyoxometalates chemistry, being of great interest in catalysis, material science and medicine [1-5]. The last thirty years have witnessed a large amount of work in order to prepare and characterize substituted Keggin polyoxotungstate species [6].

A widespread means of functionalizing polyoxometalates [1, 2] is the substitution of some of the addenda atoms with other elements. Substituting (Mo, W) with lower-valence atoms (V, Nb, Ta) has been deemed as interesting, as it leads to further oligomerization of polyoxometalates into larger structures [3,7, 8], or coordination with electrophilic moieties [9,10]. Keggin [11] type anions are the most widely studied polyoxometalates, structural information on those substituted with lower-valence atoms are well established [12-14].

Monolacunary $[PVMo_{10}O_{39}]^{8-}$, monovanado-decamolybdophosphate Keggin polyoxo- anion with mixed addenda, forms new complexes with transition metal cations, in which the metal-to-ligand ratio is 1:1. The aim of the present paper is to report the synthesis and investigation of five new complexes of the $[PVMo_{10}O_{39}]^{8-}$ ligand, with $M^{n+}$ transition metal cations ($Mn^{2+}$, $Fe^{3+}$, $Co^{2+}$, $Ni^{2+}$ and $Cu^{2+}$) with a Keggin structure and 1:1 molar ratio, which correspond to the general formula $K_{8-n}[M^{n+}(H_2O)PVMo_{10}O_{39}] \cdot xH_2O$. Complexes were investigated and characterized by FT-IR, UV-Vis, EPR spectroscopy, powder X-ray diffraction and electro-chemical measurements. This allowed the further determination of the behaviour of encapsulated transition metal ions, their coordination by Keggin fragments, the corresponding local symmetry and their structure.

## Experimental part

All chemicals were obtained from commercial sources and used without further purification. Only distilled water was used in all procedures. Elemental analysis of P, Mo, V, Mn, Fe, Co, Ni and Cu was performed on a Varrian ASA 220 type spectrophotometer. Potassium was determined by flamephotometry with an Eppendorf flame photometer. Thermal stability analyses were performed in air on a Paulik-Erdely OD-103 derivatograph (20-800°C) at 5°C $min^{-1}$. FT-IR spectra were recorded in the 400-4000 $cm^{-1}$ on a Biorad FTS 60A spectrophotometer using KBr pellets. Raman spectra were performed on solid powders at room temperature, using a DILOR OMARS 89 Raman spectrophotometer ($\lambda e$ = 1064 nm). UV-VIS spectra were recorded in the 190-1100 nm on Shimadzu UV-VIS model mini-1240 spectophotometer. EPR spectra were obtained with a Bruker ESP 380 spectrometer. X-ray diffraction (XRD) measurements were performed using a BRUKER D8 Advance X-ray diffractometer, working at 40 kV and 40 mA and the goniometer was equipped with a germanium monochromator in the incident beam. The X-ray diffraction patterns were collected in a step-scanning mode with steps of $\Delta 2\theta = 0.01°$ using Cu K$\alpha$1 radiation ($\lambda$ = 1.54056 A) in the $2\theta$ range 5-80°. Corundum powder was used as standard for instrument broadening correction.

The cyclic voltammetry measurements were carried out using a computer-controlled electrochemical analyzer (PGStat 10, AutoLab, Nederlands). The conventional three electrodes cell was equipped with a graphite working electrode (3 mm diameter, Ringsdorff, Germany), a

*email: pcorinamara@yahoo.com: Tel.:0740208485

platinum wire auxiliary electrode and an Ag/AgCl, $KCl_{sat}$ reference electrode, respectively. Before use, the working electrode was cleaned by polishing with successively finer grade emery paper and all electrochemical studies were performed at room temperature. The compounds solutions were freshly prepared just before use, by dissolving the appropriate amounts of complexes into the 0.25 M solution of $Na_2SO_4$ supporting electrolyte. The *p*H values of the solutions were adjusted using diluted $H_2SO_4$.

*Synthesis of compounds*

*$K_8[PVMo_{10}O_{39}]'$ . $16H_2O$ (**L**):* A solution containing 1.42 g (7.25 mmol) of $NaVO_3$ . $2H_2O$ solved in minimum quantity of distilled water was added dropwise with stirring to a mixture between 17.53 g(72.42 mmol) $Na_2MoO_4$ . $2H_2O$ and 1.00 g (7.25 mmol) $NaH_2PO_4$ . $H_2O$ dissolved in 50 mL distilled water. The resulting solution was stirred for 30 minutes at room temperature. When the solution cleared, the *p*H was adjusted at 4.7 with 1 M HCl solution. Any insoluble material was removed by filtration under suction and 5.00 g (67 mmol) KCl was added to the red filtrate, after which the solution was kept at 5°C for 30 min. Orange crystals of $K_8[PVMo_{10}O_{39}]$ . $16H_2O$ were obtained, which were collected and washed with 20 mL deionized water, 20 mL ethanol and 20 mL diethyl ether and then dried in a desiccator. Yield: 6.85 g (43.6 %). UV (nm): 212; 310; IR ($cm^{-1}$): 3569 s, 3489 s, 3474 s, 3186, 1624 m, 1042 w, 1031 w, 984 m, 945 vs, 929 s, 839 m, 807 m, 729 m, 690 sh, 593 w, 523 w; Raman ($cm^{-1}$): 960 vs, 889 w, 505 w, 376 w, 229 m, 150 w; Anal. Calcd. (Found): K, 14.26 (14.00); Mo, 43.73 (43.50); V, 2.32 (2.00); P, 1.41 (1.50); $H_2O$, 9.54 (9.74) %.

*$K_6[Mn(H_2O)PVMo_{10}O_{39}]$ . $10H_2O$ (**1**):* To a solution obtained by dissolving 5 g (2.30 mmol) $K_8[PVMo_{10}O_{39}]$ . $16H_2O$ in 40 mL distilled water having *p*H = 4.3 by adding 1N HCl , a solution obtained by dissolving of 0.46 g (2.30 mmol) of $MnCl_2$ . $4H_2O$ dissolved in minimum quantity of distilled water was added drop-wise under stirring. The *p*H was adjusted between 3.75-4.00 with 0.1 M HCl and 5% solution of $KHCO_3$ respectively. The mixture was kept at room temperature, 30 min under stirring. Any insoluble material was removed by filtration under suction and then to the filtrate was added 2 g (26.8 mmol) of KCl power, and kept 2-3 days at 6°C. After 3 days the red-orange crystals of $K_6[Mn(H_2O)PVMo_{10}O_{39}]$ . $10H_2O$ were filtered and washed with ethanol. The crystals were kept two days at room temperature in a desiccator. The complex was recrystallized from deionized water with *p*H 3.75 – 4.00, at room temperature. Yield: 2.6 g (49 %). UV (nm): 217, 313,5 IR ($cm^{-1}$): 3564 m, 3378 m, 1616 m, 1079 sh, 1062 w, 1045 w, 945 sh, 932 s, 870 m, 782 m, 720 m, 680 m, 643 m, 522 w; Raman ($cm^{-1}$): 1095 w, 987 s, 885 w, 229 m; Anal. Calcd (Found): K, 10.87 (10.84); Mo, 44.59 (44.72); V, 2.37 (2.20); Mn, 2.55 (2.47); P, 1.44 (1.43); $H_2O$, 9.20 (9.875) %.

*$K_5[Fe(H_2O)PVMo_{10}O_{39}]$ . $8H_2O$ (**2**):* The synthetic procedure above was followed using 0.37 g (2.30 mmol) $FeCl_3$ instead of $MnCl_2$ . $4H_2O$. The addition of KCl (2 g) to the solution led to red-orange crystals of $K_5[Fe(H_2O)PVMo_{10}O_{39}]$ . $8H_2O$, which were filtered off and dried in desiccator. Yield: 2.85 g (60.15 %). UV (nm): 218, 312; IR ($cm^{-1}$): 3470 m, 1609 m, 1080 w, 1068 w, 1051 w, 944 s, 858 m, 776 vs, 593 w; Raman ($cm^{-1}$): 995 s, 975 sh, 233 m; Anal. Calcd (Found): K, 9.38 (9.30); Mo, 46.18 (46.31); V, 2.45 (2.29); Fe, 2.69 (2.58); P, 1.49 (1.42); $H_2O$, 7.79 (7.81) %.

*$K_6[Co(H_2O)PVMo_{10}O_{39}]$ . $17H_2O$ (**3**):* The synthetic procedure above was followed using 0.53 g (2.30 mmol) $CoCl_2$ . $6H_2O$ instead of $MnCl_2$ . $4H_2O$. The addition of KCl (2 g) to the solution led to red-orange crystals of $K_6[Co(H_2O)PVMo_{10}O_{39}]$ . $17H_2O$ which were filtered off and dried in desiccator. Yield: 2.61 g (51 %). UV (nm): 212, 315; IR ($cm^{-1}$)3470 sh, 3373 m, 1617 m, 1080 w, 1068 w, 1051 w, 942 s, 887 m, 779 s, 520 w; Raman ($cm^{-1}$): 989 s, 974 s, 229 m; Anal. Calcd (Found): K, 10.25 (10.08); Mo, 42.05 (42.18); V, 2.23 (2.15); Co, 2.58 (2.46); P, 1.36 (1.33); $H_2O$, 14.19 (14.19) %.

*$K_6[Ni(H_2O)PVMo_{10}O_{39}]$ . $21H_2O$ (**4**) and $K_6[Ni(H_2O)PVMo_{10}O_{39}]'$ . $16H_2O$ (**4'**):* The synthetic procedure above was followed using 5.5 g (2.3 mmol) $NiCl_2$ . $6H_2O$ instead of $MnCl_2$‡$4H_2O$. The addition of KCl (2 g) to the solution led to red-orange crystals of polyoxometalate complex, which were filtered off and dried in desiccator. Yield: 3.1 g (58 %). UV (nm): 214, 314; IR ($cm^{-1}$): 3569 sh, 3470 sh, 3373 m, 1616 m, 1080 sh, 1062 w, 1045 sh, 945 sh, 939 vs, 874 s, 788 vs, 645 w, 518 w, 225 w; Raman ($cm^{-1}$): 991 s, 975 sh, 235 m; Anal. Calcd (Found) for **4**: K, 9.94 (9.89); Mo, 40.77 (40.89); V, 2.17 (2.02); Ni, 2.49 (2.41); P, 1.32 (1.28); $H_2O$, 16.82 (16.72) %.

*$K_6[Cu(H_2O)PVMo_{10}O_{39}]$ . $17H_2O$ (**5**):* The synthetic procedure above was followed using 0.39 g (2.3 mmol) $CuCl_2$ . $6H_2O$ instead of $MnCl_2$ . $4H_2O$. The addition of KCl (2 g) to the solution led to red-orange crystals of $K_6[Cu(H_2O)PVMo_{10}O_{39}]$ . $17H_2O$ which were filtered off and dried in desiccator. Yield: 2.0 g (38 %). UV (nm): 211, 316; IR ($cm^{-1}$): 3569 sh, 3373 m, 1617 m, 1080 w, 1062 w, 1045 w, 941 s, 872 m, 782 s, 593 w, 520 sh; Raman ($cm^{-1}$): 996 sh, 979 vs, 519 w, 235 m, 156 w, 108 w; Anal. Calcd (Found): K, 10.23 (10.20); Mo, 41.97 (42.15); V, 2.23 (2.18); Cu, 2.78 (2.62); P, 1.36 (1.33); $H_2O$, 14.16 (13.41) %.

**Results and discussions**

The thermal stability of **1-5** complexes was investigated by TG-DTG-DTA. The weight loss between 20-175°C corresponds to lattice water molecules content. The dehydration process is accompanied by two endothermic processes at ~70 and ~ 180°C as observed on the DTA curve. The second weight loss observed on the DTG curve between 270–350°C is assigned to the loss of the coordination molecule. According to the literature, the first exothermic peak of DTA curve, which usually occurs at 20–30°C after the temperature of polyoxometalate decomposing [15], is regarded as the thermal stability sign of polyoxometalates [16]. For the compounds **1-5,** the first exothermic peak appeared between 330- 360°C, indicating a good thermal stability of the complexes in following order:

**L** (276°C) < **5** (331°C) < **1** (345°C) < **2** (346.5°C) < **3** (348.5°C) < **4** (351°C)

The endothermic processes at ~430°C and ~540°C are due to oxides mixture formation and structural transformations.

FT-IR spectra of **1-5** complexes in the range of 4000-400 $cm^{-1}$ are shown in figure 1 along with those of the monolacunary Keggin ligand **L**. Comparing FT-IR frequencies of the monolacunary ligand **L** with those **1-5** complexes of the transition metal cations, we have obtained information concerning the coordination of the transition cations in the vacant position of the monolacunary polyoxometalate ligand. The similarity

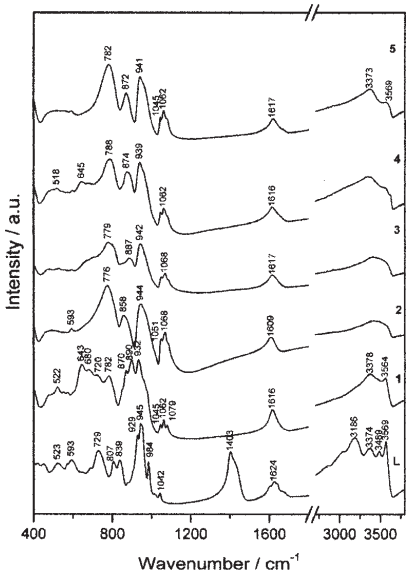


Fig. 1 FT-IR spectra of polyoxometalate compound **1-5**, comparatively with ligand **L** spectrum, in KBr pellets

between FT-IR spectra for **L** ligand and for **1-5** complexes shows that the main vibration bands are due to the polyoxomolibdate structure [17]. In the FT-IR spectrum of **L** ligand, the intense broad band at ~3374 $cm^{-1}$ is attributed to hydrogen-bonded $\nu_{as}$(OH) vibration, and in–plane δ (OH) bending appears as a medium band at 1624 $cm^{-1}$. The shoulders on the very broad $\nu_{as}$(OH) vibration band (3000-5570 $cm^{-1}$ region) are due to the coexistence of the crystallization and coordinated water molecules.

In spectra of **1- 5** complexes, the intense broad vibration band, $\nu_{as}$(OH), between 3570-3370 $cm^{-1}$, corresponds to water involved in hydrogen bonds and is due to the crystallization water, as well. The in-plane OH bending δ(OH) appears in complexes **1-5** as a medium band between 1609-1617 $cm^{-1}$ involved in hydrogen bonds with neighbouring water molecules [17]. The $\nu_{as}$(P-$O_i$), where $O_i$ is the internal oxygen atom which links P and mixed addenda of Mo and V, respectively, frequency appearing in the ligand **L** spectrum as two weak bands at 1042 $cm^{-1}$ and 1031 $cm^{-1}$, while in complexes **1-5** spectra these appearing as three weak bands, showing the presence of phosphorus as heteroatom in the polyoxometalate framework. The tiny shift of the $\nu_{as}$(P-$O_i$) anti-symmetric stretching vibrations towards higher energies in complexes **1-5** indicates that the coordination increases the cohesion of the monolacunary ligand structure around transition metal cations. Bands of stretching vibrations $\nu_{as}$(Mo-$O_t$) and $\nu_{as}$(V-$O_t$) in the ligand shown at 984 $cm^{-1}$ and 945 $cm^{-1}$, respectively, are superposed in spectra of the complexes **1-5**, and shown as broad band between 932- 944 $cm^{-1}$ [18]. The relative small shift of the $\nu_{as}$(Mo-$O_t$) stretching vibrations, either towards lower frequencies is due to the fact that the terminal $O_t$ atoms are not involved in the coordination of the transition metal cations. The two bands at 929 (vs, sp) $cm^{-1}$ and 839 (m) $cm^{-1}$, respectively, for three centers Mo-$O_c$-Mo bonds of the corner-sharing $MoO_6$ octahedron, are shown in the spectrum of the ligand and only one medium band appears in FT-IR spectra of the complexes (by 870 for **1**, 858 for **2**, 887 for **3**, 874 for **4** and 872 for **5**, $cm^{-1}$ respectively). The increase in the spectra of the complexes the $\nu_{as}$(Mo-$O_c$-Mo) frequency for the three-center bonds of corner-sharing that belongs to the cap region indicates the shortening of these bonds after the metallic ions coordination. Similarly, two vibration bands for three-center Mo-$O_e$-Mo bonds of the edge-sharing $MoO_6$ octahedron appear in the FT-IR spectra of the ligand at 807 (w) $cm^{-1}$ and 729 (m) $cm^{-1}$, respectively, suggesting that two non-equivalent bonding of this type is present. In complexes **1-5** one of them belonging to the belt region lost, but the other belonging to the cap region with the lower frequency remains (by 782 (vs) for **1**, 776 (vs) for **2**, 779 (s) **3**, 788 (s) for **4** and 782 (vs) for **5** $cm^{-1}$, respectively). The increase in the spectra of the complexes of the $\nu_{as}$(Mo-$O_e$-Mo) frequencies for the three-center bonds of edge-sharing $MoO_6$ octahedron indicates the shortening of these bonds after the metallic ion coordination and increase the symmetry and stability of these compounds. In conclusions can be said that the shift of $\nu_{as}$(Mo-$O_c$-Mo) and $\nu_{as}$(Mo-$O_e$-Mo) frequencies for the bonds from the cap region of the monovacant Keggin units, shows the coordinate of each transition metallic ion by the oxygen atoms from corner-sharing and edge-sharing octahedron.

Raman spectra of **1-5** complexes in the 1200-100 $cm^{-1}$ are shown in figure 2 comparatively with those of the monolacunary Keggin ligand **L**. The Raman spectrum of the ligand shows the three characteristic bands at 960 (vs) $cm^{-1}$, 889 (m) $cm^{-1}$ and 229 (m) $cm^{-1}$, assigned to $\nu_s$(Mo-$O_t$), $\nu_{as}$(Mo-$O_t$) and $\nu_s$(Mo-$O_i$), respectively. These bands are shifted in the Raman spectra of the complexes (at 987 (s), 885(sh) and 229 (w) $cm^{-1}$ for **1**, 995 (s), 975 (sh) and 233 (w) $cm^{-1}$ for **2**, 989 (s), 974 (s) and 229 (w) $cm^{-1}$ for **3**, 991 (s), 975 (sh) and 235 (w) $cm^{-1}$ for **4**, and 996 (sh), 979 (vs) and 235 (m) $cm^{-1}$ for **5**, respectively). In Raman spectra, the bands assigned to vibrations of the complexes **1-5**, Mo-$O_t$ bonds were shifted towards higher energies, comparatively with the ligand. This suggests higher stability of the complexes [19, 20].

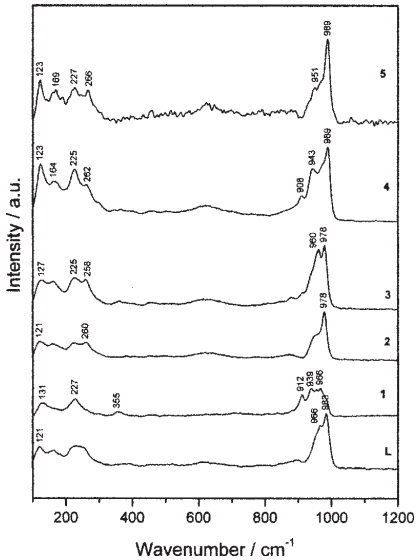


Fig. 2 Raman spectra of polyoxometalate compounds **1-5,** comparatively with ligand **L** spectrum, in powder

The electronic UV and Vis spectra were registered on aqueous solutions of the potassium salts of the complexes **1-5** and compared with those of the ligand or with the hexaaqua complexes of the $Mn^{2+}$, $Fe^{3+}$, $Co^{2+}$, $Ni^{2+}$ and $Cu^{2+}$ in octahedral field [21].

UV spectra of polyoxometalate clusters generally exhibit two charge-transfer (CT) bands, characteristic to the polyoxoanionic framework, which are ascribed to oxygen-to-metal transitions. In UV spectrum of the ligand **L,** the broad $\nu_1$ CT band, due to $d_\pi$-$p_\pi$-$d_\pi$ transitions from the three-center Mo-$O_{c,e}$-Mo and Mo-$O_{c,e}$-V bonds recorded at 321 nm/31150 $cm^{-1}$. The sharper $\nu_2$ CT band, due to dπ-pπ transitions of the Mo=$O_t$ and V=$O_t$ bonds, have the maximum detected at 209 nm/47850 $cm^{-1}$. The UV

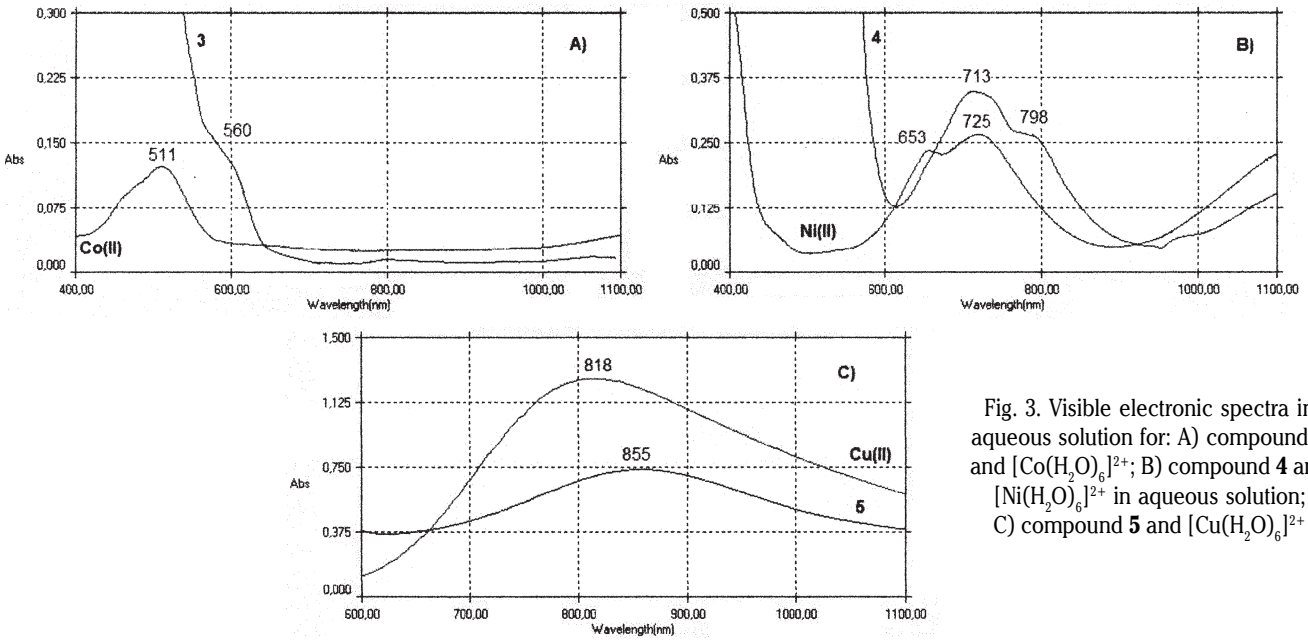


Fig. 3. Visible electronic spectra in aqueous solution for: A) compound **3** and $[Co(H_2O)_6]^{2+}$; B) compound **4** and $[Ni(H_2O)_6]^{2+}$ in aqueous solution; C) compound **5** and $[Cu(H_2O)_6]^{2+}$

spectra of the ligand and complexes are also similar, proving that the charge transfer inside in polyoxometalate structure is not significantly affected by coordination. The lower energy band $\nu_1$ was shifted to higher frequencies in complexes spectra, compared to the ligand, and this is due to the increase of the symmetry, of the $MoO_6$ and $VO_6$ octahedron through coordination, which influences the electronic transfer from these bonds. The higher energy band $\nu_2$ was shifted to lower frequencies in complexes spectra, compared to the ligand, and this is due to the decrease of the symmetry, of the $MoO_6$ and $VO_6$ octahedron through coordination, which influences the electronic transfer from these bonds [22].

Visible spectra only show electron transfer bands of the $M^{n+}$ transition metal ions coordinated by the ligand. However, the expected transition bands are not found in the spectrum of complex **1** and **2**. The very low intensity d-d transitions of the ($d^5$) $Fe^{3+}$ and $Mn^{2+}$ ions, forbidden by the Laporte and spin selection rules, are totally masked by the $\nu_1$ charge transfer band, which extends from UV into the visible range [21]. This indicates that $Fe^{3+}$ and $Mn^{2+}$ ions are involved in the charge transfer in complexes **1** and **2.**

The absorption bands of the **3-5** complexes recorded in the visible range were compared to those of the corresponding $[Co(H_2O)_6]^{2+}$, $[Ni(H_2O)_6]^{2+}$ and $[Cu(H_2O)_6]^{2+}$ aqua-cations in octahedral field conform to literature [21, 22]. The Vis spectrum of complex **3** (fig. 3A) shows the characteristic features of $Co^{2+}$ ($d^7$) ion in a distorted octahedral environment: show a band at 550 nm/18180 $cm^{-1}$ with a shoulder at 630 nm/15870 $cm^{-1}$ corresponding to the $^3A_{2g}(F) \rightarrow {}^3T_{1g}(F)$ ($\nu_2$) and $^4A_{2g} \leftarrow {}^4T_{1g}$ transitions.

The Vis spectrum of complex **4** (fig. 3B) shows the characteristic features of $Ni^{2+}$ ($d^8$) ion in a distorted octahedral environment: show two bands at 713 nm/14025 $cm^{-1}$ and 798 nm/12530 $cm^{-1}$ corresponding to the $^3A_{2g}(F) \rightarrow {}^3T_{1g}(F)$ and $^3A_{2g}(F) \rightarrow {}^3T_{1g}(P)$ transitions.

The visible spectrum of the complex **5** (fig. 3C) presents a broad absorption curve with a maximum at approximately 855 nm/11700 $cm^{-1}$ suggesting a distorted octahedral environment around the $Cu^{2+}$ ($d^9$) ion. This band can be attributed to the $^2E_g \rightarrow {}^2T_{2g}$ transition. Three transition are expected ($d_{xy}$, $d_{yz} \rightarrow d_{x^2}$ and $d_{xy} \rightarrow d_{x^2-y^2}$), but these are very close in energy and give rise to a single asymmetric broad band. The greater shift in the case of the copper ion in the complex **5**, as opposed to the aqua copper complex associated with the band asymmetry can be traced back to the Jahn-Teller distortion.

In EPR spectra of the complexes **1, 3** and **4** the signals of the vanadium ions from ligand overlap the signals of the $Mn^{2+}$, $Co^{2+}$ and $Ni^{2+}$ ions. Although the signals of the vanadium ions are present in the spectrum of the compound **2** too, this spectrum can be interpreted.

EPR spectra of the compounds **2** and **5** were interpreted by considering the octahedral geometry of the $Fe^{3+}$ and $Cu^{2+}$ into monolacunary $[PVMo_{10}O_{39}]^{8-}$ ligand, and were discussed by considering noninteracting $Fe^{3+}$ and $Cu^{2+}$ ions, respectively. The powder EPR spectrum obtained in the X-band at room temperature for complex **2** (fig. 4A) contains three main feature at the effective g values at 7.942, 4.265 and 1.997 specific for $Fe^{3+}$ ions. Hyperfine structure of lines with axial symmetry, characteristic for vanadium ion addenda, was solved in $g \approx 2$ area. The EPR spectrum of compound **2** exhibits a broad signal at $g_{eff} \approx 4.265$, which corresponds to the high state S=5/2 of $Fe^{3+}$. Also, the g value ($g_{eff} \approx 7.942$), greater than 6.0 indicates that at this temperature the complex **2** is characterized by one $S \geq 5/2$ spin state [23, 24].

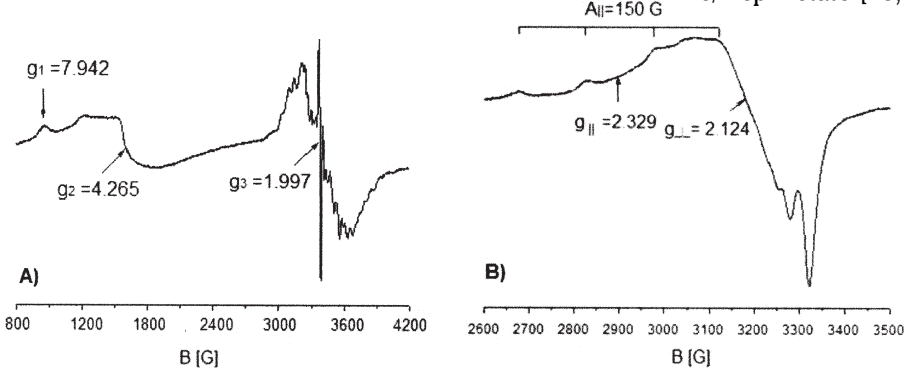


Fig. 4. Powder EPR spectra recorded in the X-band at room temperature for: A) compound **2**; B) compound **5**

Four lines with metallic hyperfine structure are included in EPR spectrum of copper complex **5** (fig.4.B), both parallel and in perpendicular bands. The powder EPR spectrum of compound **5** was discussed by considering non-interacting $Cu^{2+}$ ions, $g_{||} = 2.329$, $g_{\perp} = 2.124$ principal gyromagnetic values and $A_{||} = 150$ G, line widths. These values indicate an axial symmetry around the $Cu^{2+}$ ions [25]. The powder EPR spectra, of the compounds **2** and **5**, obtained in the X band at room temperature are typical for mononuclear species.

Figure 5 shows the XRD patterns of the α-Keggin monovanado-decamolybdophosphate investigated powders. The XRD diffraction patterns illustrates the fact that the **4, 4'** and **5** investigated compounds obtained in our synthesis conditions are single phase materials containing mainly the α-Keggin monovanado-decamolybdophosphate monoclinic $P2_1/c$ structure phase [26]. Both crystallization ability with a different number of water molecules and the efflorescence phenomenon are specific properties of Keggin polyoxometalates and justifies getting the same structural type for **4** and **4'**, which are coordination compounds of $Ni^{2+}$ with **L** [1, 27]. The intense peak at 2θ = 9.4° in the XRD pattern seems to indicate that the compound may have layered type of structure [28].

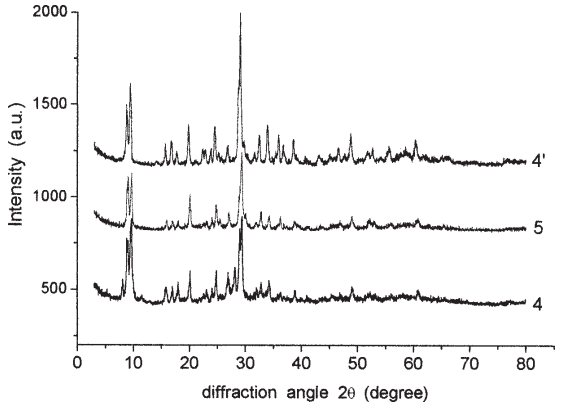


Fig 5. X-ray powder diffraction patterns for compounds **4**, **5** and **4'**

The Rietveld calculation provides the crystallographic information by comparing the model profile with X-ray or neutron curves using the least squares method. One uses Rietveld analysis generally to get the lattice parameters, atomic positions and atomic distances [29]. The peak positions of X-ray diffraction curve are related to the unit cell lattice constants of the crystal structure and peak intensities are affected by various parameters such as atomic position, atomic occupancy, and thermal effect. Rietveld method based on pseudo-Voigt profile fitting function was applied to perform a simultaneous refinement of X-ray diffraction patterns concerning both material structure and microstructure. Microstructural informations obtainable by the X-ray Rietveld refinement method consist of effective crystallite mean size, $D_{eff}$ *(nm)* and the root mean square (rms) of the microstrains, $<\varepsilon^2>^{1/2}$m [30]. The Rietveld refinement of the X-ray diffraction data has been done using the PowderCell software [31].

To simulate the X-ray powder diffraction patterns of the α-Keggin molybdophosphates monoclinic structure, the space group $P2_1/c$ (*SG 14*) was used as input parameters. The background of each pattern was fitted by a fourth order polynomial function. First, the background was refined; the positions of the peaks were corrected for zero-shift error by successive refinements and then the structural and microstructural parameters were refined. The unit cell parameters, the effective crystallite mean size, $D_{eff}$ (nm), the root mean square (rms) of the microstrains, $<\varepsilon^2>^{1/2}$m and profile (Rp) discrepancy indices at their reached minimum values calculated by Rietveld refinement analysis using PowderCel computer program for the investigated samples are presented in table 1.

The electrochemical behaviour of compounds **2** and **5**, was studied by recording cyclic voltammograms in 0.25 M solution of $Na_2SO_4$ (*p*H 2.5 or 5.1) (fig. 6A and 6B). For compound **5**, in the potential range of -1.5 to 1 V, voltammograms reveal the appearance of some consecutive waves placed at $E_{pa,1} = 0.34$ and $E_{pc,1} = 0.15$; $E_{pc,2} = -0.40$ and $E_{pc,3} = -0.95$ V *vs.* Ag/AgCl,$KCl_{sat}$ (at *p*H 2.5 and scan rate 25 mV/s) as presented in literature for similar compounds [32, 33].

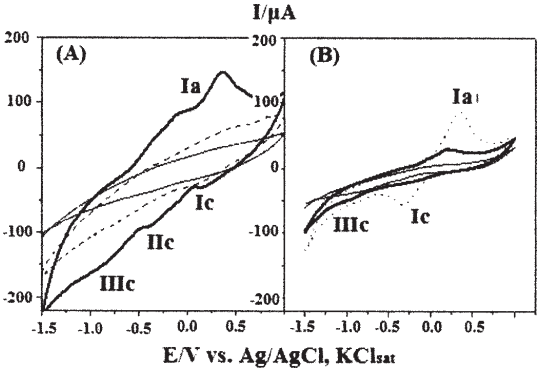


Fig. 6. Cyclic voltammograms of $10^{-3}$M compound **5** (thick solid line, A and B), $10^{-3}$M complex **2** (dot line, A) and $10^{-3}$M compound **5** + $10^{-3}$ M $CuSO_4$ (dot line, B) on graphite electrode. Experimental conditions: electrolyte, $Na_2SO_4$ 0.25 M (thin solid line, A and B), pH 2.5 (A), *p*H 5.1 (B); scan rate, 25 $mV*s^{-1}$; starting potential, -1.5 V *vs.* Ag/AgCl, $KCl_{sat}$

The quasi-reversible (wave I) or irreversible (wave II and III) redox processes are supposed to correspond to the behaviour of Cu(II) → Cu(0) (wave $I_a/I_c$), or to the reduction of V and Mo ions from phosphovanadomolybdate structure (waves IIc and IIIc, respectively) [34, 35].

The compound **2** presents a similar behaviour with the **5** compound; the redox behaviour of iron ions being covered by the other processes (fig. 6A). At *p*H 5.1, the cathodic scan of compound **5** reveal only two waves placed at $E_{pc,1} = -0.40$ and $E_{pc,2} = -0.95$ V *vs.* Ag/AgCl,$KCl_{sat}$ (at *p*H 5.1 and scan rate 25 mV/s), probably due to a

**Table 1**

UNIT CELL PARAMETERS OF THE α-KEGGIN MOLYBDOPHOSPHATES - MONOCLINIC PHASE, THE EFFECTIVE CRYSTALLITE MEAN SIZE, $d_{eff}$ (nm), THE MEAN ROOT MEAN SQUARE (rms) OF THE MICROSTRAINS , $<\varepsilon^2>^{1/2}$m AND PROFILE (rp) DISCREPANCY INDICES CALCULATED BY RIETVELD REFINEMENT ANALYSIS FOR THE INVESTIGATED SAMPLES

| Compound | Chemical composition | a | b | c | β | V $10^3$ | $D_{eff}$ | $<\varepsilon^2>$ | $R_p$ |
|---|---|---|---|---|---|---|---|---|---|
| | | [nm ] | [nm ] | [nm ] | [deg] | $[nm]^3$ | [nm ] | $^{1/2}$m $10^3$ | |
| 4 | $K_6[NiPVMo_{10}O_{39}]\cdot 21H_2O$ | 0.93632 | 2.03666 | 1.16908 | 93.45 | 2.22559 | 15.2 | 0.574 | 26.4 |
| 4' | $K_6[NiPVMo_{10}O_{39}]\cdot 16H_2O$ | 0.93053 | 2.03106 | 1.16077 | 93.18 | 2.19006 | 29.2 | 0.104 | 26.5 |
| 5 | $K_6[CuPVMo_{10}O_{39}]\cdot 17H_2O$ | 0.93449 | 2.03566 | 1.16503 | 93.34 | 2.21249 | 20.6 | 0.273 | 28.3 |

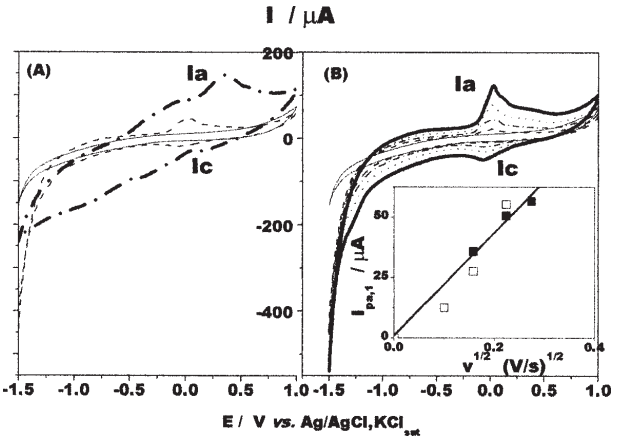


Fig. 7 The influence of the *p*H (A) and of the scan rate (B) of $10^{-3}$M compound **5** on graphite electrode. Inset: I *vs.* $v^{1/2}$ dependence at pH 2.5 (■) and *p*H 5.1 (□). Experimental conditions: electrolyte, $Na_2SO_4$ 0.25 M, *p*H 2.5 (thin solid line and dash dot line on A and all lines on B), *p*H 5.1 (dash line on A); scan rate, 10 mV $s^{-1}$ (dash line B), 25 mV $s^{-1}$ (all line on A, dash dot line on B), 50 mV $s^{-1}$ (dot line on B), 100 mV $s^{-1}$ (thick solid line on B); starting potential, -1.5 V vs. Ag/AgCl, $KCl_{sat}$

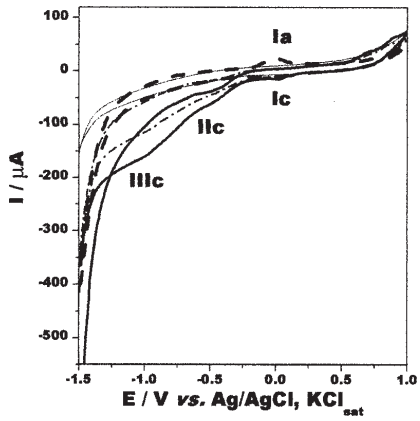


Fig. 8 The electrocatalytic effect of $10^{-3}$M compound **5** (dash line) on 0.02 M (dash dot line) and 0.04 M (thick solid line) $H_2O_2$ electroreduction at graphite electrode. Experimental conditions: electrolyte, $Na_2SO_4$ 0.25 M, *p*H 5.1 (thin solid line); scan rate, 10 mV*$s^{-1}$; starting potential, -1.5 V *vs.* Ag/AgCl, $KCl_{sat}$

superposition of the Cu on the Mo or V behaviour (fig. 6B). In order to identify the contribution of the $Cu^{2+}$ ions, on the redox response of compoud **5**, increasing volumes of 1 mM $CuSO_4$ were added to 1 mM compound **5** solution, and the corresponding cyclic voltammograms were recorded in figure 6B. In the experimental done conditions, the addition of $CuSO_4$ leads to a significant increase of the $I_{pa,1}$ and $I_{pc,1}$ peaks current.

Generally, the reduction of the polyoxometalates is accompanied by protonation, therefore in figure 7A, it can be observed that as expected, the increase of the electrolyte *p*H value lead to a negative shift of recorded cyclic voltammograms. The influence of the scan rate on the redox behaviour of compound **5** is show in figure 7B. It is worth to underline that, the slopes of the log–log dependence between the peak currents and the potential scan rate for the peak $I_a$ of the complex **5** are equal to 0.38 ± 0.05 A/(V $s^{-1}$) (R = 0.9845, n = 4) and 0.85 ± 0.05 A/(V $s^{-1}$) (R = 0.9973, n = 4) at *p*H 2.5 and *p*H 5.1, respectively. In spite of the fact that at *p*H 5.1, the absorption of the complex on the electrode surface is not negligible, the electrochemical activity of **5** could be considered as mixed ones, being both diffusion- and surface-controlled [36]. Also, despite the fact that the background current at *p*H 2.5 is greater than at pH 5.1, the anodic current intensity of peak $I_a$ has similar values both at *p*H 2.5 and *p*H 5.1 ( fig. 7B).

The easy, rapid and safe detection of micromolar to millimolar concentrations of $H_2O_2$ is of great importance, because it is confirmed that exposure to $H_2O_2$ at levels greater than 50 μM is cytotoxic for an extensive variety of bacterial cells in culture, animals and plants [35].To avoid high overpotential of the oxidation/reduction of $H_2O_2$ on conventional electrodes (gold, graphite), enzymatic and non-enzymatic modified electrode are currently used. The non-enzymatic mediated pathway includes modified electrodes with nanostructured metal oxides [37, 38], nanocomposites based on carbon nanotubes [39, 40], conjugated polymer [41, 42], or Keggin-type polyoxometalates [43, 44]. The electrocatalytic activity of compound **5** on the $H_2O_2$ reduction at a graphite electrode is presented in figure 8. The electrocatalysis occurs at peaks $II_c$ and $III_c$; the intensity of these peak currents increases with the increase of the $H_2O_2$ concentration, while the intensity of peak $I_c$ is unaffected by the presence of $H_2O_2$.

## Conclusions

This work reports the synthesis and characterization of the potassium salt of the monosubstituted α-Keggin monovanado-decamolybdophosphate with $Mn^{2+}$, $Fe^{3+}$, $Co^{2+}$, $Ni^{2+}$ and $Cu^{2+}$ cations, a very interesting category of compounds, because of the catalytic and biologic properties of the vanadium element.

The complexes were synthesized in aqueous solution, by the direct addition of transition metal cations to a solution of the monolacunary Keggin polyoxo-monovanado-decamolybdophosphate anion. Elemental analysis is in good agreement with calculated values for general formula of $K_{8-n}[M^{n+}(H_2O)PVMo_{10}O_{39}]. xH_2O$.

The IR spectra show that the $K_8[PVMo_{10}O_{39}] . 16H_2O$ act as pentadentate ligand with octahedric coordination involving the oxygen atoms from corner-sharing and edge-sharing octahedron of monolacunary cavity and the oxygen atom from one water coordination molecule.

Visible electronic and EPR spectra indicate $O_h$ local symmetry for transition metal cations in studied compounds.

The XRD patterns of $K_6[Ni(H_2O)PVMo_{10}O_{39}] . xH_2O$ (x = 16, 21) and $K_6[Cu(H_2O)PVMo_{10}O_{39}] . 17H_2O$ salts show that the complexes crystallized in monoclinic system, space group $P2_1/c$ and change both the number of crystallization water molecules and metal cation coordinated led only to change the unit cell parameters.

The preliminary electrochemical behaviour of compound $K_6[Cu(H_2O)PVMo_{10}O_{39}] . 17H_2O$ investigated at different scan rate and different *p*H values exhibited successively quasi-reversible (peak $I_a/I_c$) and irreversible (peaks $II_c$, $III_c$) waves. The redox processes attributed to peak $I_a/I_c$ is a mixed ones, being both diffusion- and surface-controlled and sensitive at the *p*H of solution. The electroreduction of $H_2O_2$, electrocatalysed by both Mo and V ions of compound $K_6[Cu(H_2O)PVMo_{10}O_{39}] . 17H_2O$, was also evidenced and is revealing potential applications of the compound as electrocatalyst and electron transfer device.

## References

1. POPE M.T., Heteropoly and Isopoly Oxometalates, Springer-Verlag: Berlin, 1983.

2. POPE M. T., MÜLLER A., Angew. Chem. Int. Ed. Engl., **30**, 1991, p. 34.
3. RUHLE J.T., HILL C.L., JUDD D.A., SCHINAZI R.F., Chem. Rev., **98**, 1998, p. 327.
4. POPE M. T., MÜLLER A., Polyoxometalates: from Platonic Solids to Anti-Retroviral Activity; Eds. Kluwer, Dordrecht, Netherlands, 1994.
5. BAKER L.C.W., Plenary Lecture, Proc. XV Int. Conf. Coord. Chem. Moscow, 1973.
6. BAKER L.C.W., GLICK D., Chem. Rev., **98**, 1998, p. 3 (and references therein).
7. YAMASE T., OZEKI T., SAKAMOTO H., NISHIYA S., YAMAMOTO A., Bull. Chem. Soc. Jpn., **66**, 1993, p.103.
8. LIN Y., WEAKLEY T.J.R., RAPKO B., FINKE R.G., Inorg. Chem., **32**, 1993, p. 5095.
9. SAKAI Y., YOZA K., KATO C.N., NOMIYA K., J. Chem. Soc. Dalton Trans., 2003, p. 3581.
10. KLEMPERER W.G., YAGASAKI A., Chem Lett., 1989, p. 2041.
11. KEGGIN J.F., Nature, **131**, 1933, p. 908.
12. KAWAFUNE I., TAMURA H.. MATSUBAYASHI G., Bull, Chem. Soc. Jpn., **70**, 1997, p. 2455.
13. DAVID L., CRACIUN C., RUSU M., RUSU D., COZAR O., J. Chem. Soc. Dalton Trans., 2000, p. 4374.
14. NOMIYA K., HASEGAWA T., NOGUCHI R., NOMURA K., TAKAHASHI M., YOKOYAMA H., Chem. Lett., 2001, p. 1278.
15. BOULTIF A., LOUER D., J. Appl. Cryst., **37**, 2004, p. 724.
16. WU Q., WANG E., LIU J., Polyhedron, **12**, 1993, p. 2563.
17. SUN G., FENG J., WU H., PEI F., FANG K., LEI H., J. Magm. Magn. Mat., **281**, 2004, p. 405.
18. MASSART R., CONTANT C., FRUCHART J.M., CIABRINI J.P., FOURNIER M., Inorg. Chem., **16**, 1977, p. 2916.
19. THOUVENOT R., FOURNIER M., FRANCK R., ROCCHICCIOLI-DELTCHEFF C., Inorg. Chem., **23**, 1984, p. 598.
20. ROCCHICCIOLI-DELTCHEFF C., FOURNIER C., FRANCK M., THOUVENOT R., Inorg. Chem., **22**, 1983, p. 207.
21. LEVER A.B.P., Inorganic Electronic Spectroscopy, Elsevier, New York, 1984.
22. SO H., POPE M.T., Inorg. Chem., **11**, 1972, p. 1441.
23. HOFF A. J., Advanced EPR. Applications in Biology and Biochemistry, Elsevier, Amsterdam, 1989.
24. STAPLES C.R., DHAWAN I. K., FINNEGAN M. G., DWINELL D. A., ZHOU Z. H., HUANG H., VERHAGEN M. F. J. M., ADAMS M. W. W., JOHNSON M. K., Inorg. Chem., 36, 1997, p. 5740.
25. BENCINI A., GATEEESCHI D., Electron Paramagnetic Resonance of Exchange Coupled Systems, Springer, Berlin, 1990.
26. ROSNES M. H., YVON C., DE-LIANG L., CRONIN L., Chem. Soc. Dalton Trans., 41, no. 33, 2012, p. 10071.
27. TSIGDINOS G., HALLADA C., Inorg. Chem., 7, no. 3, 1968, p. 437.
28. RAJKUMAR T., RANGA RAO G., J. Chem. Sci., 120, no. 6, 2008, p. 587.
29. RIETVELD H.M., J. Appl. Cryst., 2, 1969, p. 65.
30. VAN BERCUM J.G.M., VERMEULEN A.C., DELHEZ R., DE KEIJSER T.H., E.M. MITTEMEIJER, J. Appl. Phys., 27, 1994, p. 345.
31. KRAUS W., NOLZE G., J. Appl. Crystallogr., 2, 1996, p. 301.
32. TANGESTANINEJAD S., MIRKHANI V., MOGHADAM M., MOHAMMADPOOR-BALTORK I., SHAMS E., SALAVATI H., Ultrasonics Sonochemistry, 15, 2008, p. 438
33.TANGESTANINEJAD S., MOGHADAM M., MIRKHANI V., MOHAMMADPOOR-BALTORK I., SHAMS E., SALAVATI H., Catalysis Communications, **9**, 2008, p. 1001.
34. HAN D. M., GUO Z. P., ZENG R., KIM C. J., MENG Y. Z., LIU H. K., International Journal of Hydrogen Energy, **34**, 2009, p. 2426.
35. PAPAGIANNI G. G., STERGIOU D. V., ARMATAS G. S., KANATZIDIS M. G., PRODROMIDIS M. I., Sensors and Actuators B, **173**, 2012, p. 346.
36. BARD A. J., FAULKNER L. R., Electrochemical Methods, Wiley-VCH, New York, 1980, p.522.
37. SCANDURRA G., ARENA A., CIOFI C., SAITTA G., Sensors, **13**, 2013, p. 3878.
38. SONG M. J., HWANG S. W., WHANG D., Talanta, **80**, 2010, p. 1648.
39. LUO L., LI F., ZHU L., ZHANG Z., DING Y., DENG D., Electrochim. Acta., **77**, 2012, p.179.
40. ZHANG J., GAO L., Mater. Lett., **17**, 2007, p. 3571.
41. WEN Z., CI S., LI J., J. Phys. Chem., **113**, 2009, p. 13482.
42. LI Y., CHANG Y., JIN M., LIU Y., HAN G., J. Appl. Polym. Sci., **126**, 2012, p. 1316.
43. NARANG J., CHAUHAN N., PUNDIR C. S., Analyst., **136**, 2011, p. 4460.
44. FOSTER K., BI L., MC CORMAC T., Electrochimica Acta, **54**, 2008, p. 868

Manuscript received: 5.06.2013